Tribology International 145 (2020) 106177

Contents lists available at ScienceDirect

Tribology International

journal homepage: http://www.elsevier.com/locate/triboint

Microstructure and tribological behavior of *in situ* synthesized (TiB+TiC)/Ti6Al4V (TiB/TiC=1/1) composites

Bowen Zheng [a,1], Fuyu Dong [a,1,*], Xiaoguang Yuan [a,**], Hongjun Huang [a], Yue Zhang [a,***], Xiaojiao Zuo [a], Liangshun Luo [b], Liang Wang [b], Yanqing Su [b], Weidong Li [c], Peter K. Liaw [c], Xuan Wang [d]

[a] School of Materials Science and Engineering, Shenyang University of Technology, Shenyang, 110870, China
[b] School of Materials Science and Engineering, Harbin Institute of Technology, Harbin, 150001, China
[c] The Department of Materials Science and Engineering, The University of Tennessee, Knoxville, TN, USA
[d] School of Materials Science and Engineering, Chongqing University, Chongqing, 400044, China

ARTICLE INFO

Keywords:
Titanium matrix composite
Microstructure
Tribological behavior
Transfer layer

ABSTRACT

To enhance wear properties of titanium alloys, *in situ* titanium matrix composites (TMCs) were synthesized by a melting cast method with (TiC + TiB) volume fractions of 0, 2, 4, 6, 8, and 10%. The results indicated that tribological properties of TMCs were increased owing to the dispersed distribution of (TiC + TiB) reinforcements, which improved the ability to resist the surface shear stress. Moreover, the stable transfer layer formed during wear reduced the shear strength and limited the direct interaction at tribo-pair interfaces to enhance surface hardness and wear resistance effectively. Consequently, the wear mechanism appeared to transitioned from the severe adhesive and oxidative wear gradually to the slight adhesion, abrasive, and oxidative wear along with reinforcements content increased.

1. Introduction

Titanium alloys have been broadly applied in the industrial production on account of their many excellent properties, but their low surface strength and poor abrasion resistance still limit their utilization under dry sliding and severe wear conditions [1–3]. To improve their wear resistance, surface modifications such as nitriding, thermal oxidation, and spray coating have been widely adopted [4–7], however, surface modifications usually take place at thicknesses less than 100 μm, such that the modification layer is soon depleted under high speeds and loads, furthermore, this method can not improve the overall hardness and strength of materials. Therefore, it is imperative to conceive and develop appropriate means to increase the wear resistance of titanium alloy to warrant their hardness and durability in usages.

Many researches [8–11] have indicated that the *in-situ* synthesis of discontinuously reinforced TMCs is considered as a feasible process to significantly widen their utilization at high temperature, which possesses simple and low-cost preparation process, and ensures a good interfacial bonding between matrix and reinforcements. In the previous studies, SiC, TiC, TiB, TiB_2, Al_2O_3, and BN reinforcements are often seen as effective reinforced options to improve alloy stiffness, strengths, and properties at elevated temperatures [12–14]. As representative reinforcements, the TiB whiskers and TiC particles are generally regarded as the best candidates of TMCs, due to the high elastic modulus and hardness, outstanding thermal stability, similar coefficient of thermal expansion and density with Ti matrix. Due to their excellent properties, these TMCs have been gradually accepted and implemented in some industries. For instance, Toyota Motor has exploited the powder metallurgy of TiB reinforced TMCs for air-evacuation valves and inlet valves, connecting rod bearing bush, and other automobile engine parts [15]. Al die-casting sleeve assemblies adopting (TiB + TiC) reinforced TMCs exhibited better lifetime, energy efficiency, and durability compared to their Al melt counterparts [16].

For TMCs, many studies [17–19] have reported their mechanical

* Corresponding author.
** Corresponding author.
*** Corresponding author.
E-mail addresses: dongfuyu@sut.edu.cn (F. Dong), yuanxg@sut.edu.cn (X. Yuan), yuezhang@sut.edu.cn (Y. Zhang).
[1] Contributed equally to this work.

https://doi.org/10.1016/j.triboint.2020.106177
Received 19 November 2019; Received in revised form 8 January 2020; Accepted 10 January 2020
Available online 11 January 2020

properties (e.g., tensile, fatigue, and creep) and process technologies (e.g., extruding, forging, and powder metallurgy), for instance, Geng et al. have studied that the (TiB + TiC)/pure Ti matrix composites with the ratio of 1:1 gain better tensile properties over the composites with other ratios [20,21], Zhang et al. have reported the hot deformation behavior and microstructure evolution mechanism of 5 vol% (TiB + TiC)/Ti–6Al-2.5Sn–4Zr-0.7Mo-0.3Si composites with the ratio of 1:1 [22], but limited attention is paid to the wear mechanisms and characteristics of particulate-reinforced TMCs in use. Moreover, TMCs are usually applied in severe environments, such as high pressure and high temperature, so they are more vulnerable to wear damage. Therefore, it is essential to understand the wear behavior of TMCs under dry sliding and severe wear conditions. In view of published work, our group has been studied the influence of counterface materials on the friction performance of (TiC + TiB) hybrid reinforced Ti6Al4V composites [23]. Liaquat et al. have conducted a detailed study on the effect of TiC particle reinforcements and sintering parameters on the tribological properties of TiAl metal matrix composite (TMMC) and compared them with common gray cast irons to evaluate their applications as a brake disc material [24]. Blau et al. have studied the TiB or TiC-reinforced TMCs in brake disks of motor vehicles and heavy-duty trucks, owing to their outstanding properties, such as the abrasion resistance, strong stiffness, and fine corrosion resistance to road salts [25]. To summarize, TMCs have lighter weight, better stiffness, higher strength, more excellent salt corrosion resistance than comparably sized cast iron parts, which are suitable for brake discs. Therefore, *in situ* TMCs are expected to be the choice of a potential of brake disc materials. Furthermore, the wear and friction is identified as a very complicated process, which is not only related to friction conditions but also material structures [26–29]. Some researches have suggested that the changes in wear-surface hardness and temperatures are the leading factors of wear resistance [30–34]. By now, the understanding of the tribological behavior and wear mechanism of hybrid reinforced TMCs is still quite limited. Thus, it is urgent to deeply study the sliding wear behavior of hybrid reinforced TMCs with the rapid development in engineering applications. In addition, considering the requirements of brake discs and the actual application environments of TMCs, it is essential to design the compositions of TMCs, study the tribological behaviors of the composites under high-speed and high-stress conditions, and reveal their relationships with the matrix microstructures as well as the morphology and volume fraction of the reinforcement phase.

In this paper, TMCs were prepared by the *in situ* synthesis using boron carbide (B_4C) and carbon powders and Ti6Al4V as raw materials. The *in situ* reactions include $5Ti + B_4C \rightarrow 4TiB + TiC$ and $Ti + C \rightarrow TiC$. For good insights into the influence of the reinforcement volume fraction on the microstructure and tribological behavior of TMCs against the forged steel of Cr12MoV, the microstructure, transfer layer formed on the worn surface of pins, and reinforcement fracture on the cross section of worn surface were investigated.

2. Experimental procedures

The B_4C powders (98% purity, mean particle size = 50 μm) and C powders (99.8% purity, mean particle size = 5–7 μm) were mixed into the Ti6Al4V alloy to synthesized (TiB + TiC)/Ti6Al4V composites. The volume fractions of *in situ* (TiB + TiC) with a 1/1 ratio reinforced TMCs were 0, 2, 4, 6, 8, and 10%. In *situ* reactions, $5Ti + B_4C \rightarrow 4TiB + TiC$ and $Ti + C \rightarrow TiC$, were carried out using a nonconsumable arc-melting process with the argon protection. To obtain uniform structures, the smelting-casting process was repeated more than 4 times, and the melt was finally cooled in a water-cooled copper crucible. A pin-on-disc friction test apparatus (MMU-5G, Sida Tester Co. Ltd., Jinan, China) was used to conduct the dry friction tests with the forged steel of Cr12MoV (58-60HRC) as the friction pair. A 100 N load (equal to the average contact stress of 8 MPa) was applied on Φ4 × 15 mm samples for 30 min at a sliding speed of 0.11 m/s. To guarantee the stability and accuracy of the experimental data, each test was repeated three times. All specimens were subjected to an ultrasonic cleaning machine in acetone to remove residual abrasive particles on worn surfaces. The wear volume (V) was calculated by dividing the weight difference by the sample density. The sample weights before and after wear were measured by the electronic analysis balance JA5003 (the accuracy was 0.001 g), and the density was measured by the Archimedes drainage. Then, the specific wear rates of pins were obtained with the following equation:

$$W = \frac{V}{FS} \tag{1}$$

where W is the specific wear rate, V (mm^3) is the wear volume of pins, S (mm) is the total sliding distance, and F represents the normal load (N). The microstructure, phase identification, surface morphology, and element distribution of worn surfaces were detected by utilizing a Hitachi S–3400 N type scanning electron microscope (SEM; Hitachi High-Technologies Corp., Tokyo, Japan), a Shimadzu XRD-7000 type X-ray diffractometer, and a Shimadzu EPMA-1720 type electron probe micro-analyzer (Shimadzu Corp., Kyoto, Japan). The hardness of the tribo-layer and matrix was tested using a digital hardness tester (HVS-1000 type, Time-top, technology Co., Ltd., Beijing, China) with a load of 0.5 N for a sustained time of 15 s. The grain boundary and morphology of the composites were identified by the electron back-scattered diffraction (EBSD, ZEISS, GeminiSEM 300). The grain boundaries and sizes of phases were obtained by the Channel 5 HKL suite of programs (Oxford Instruments Inc., U.K.).

The chemical constituents of the wear surface of pins were determined by the X-ray photoelectron spectroscopy (XPS, ThermoFisher K-Alpha、ESCALAB 250Xi) with a mono-chromatic Al K_α source at 72 W. The XPS analysis was tested under a base pressure of 8×10^{-8} Pa, and the inspection depth was about 10 nm. The pass energy for the XPS test was set as 150 eV for wide spectrum scans and 20 eV for narrow spectrum scans, respectively. The C 1s peak value of 284.6 eV was conducted as calibrated reference.

3. Results

3.1. Microstructural evolution

Fig. 1 indicates the X-ray diffraction analysis of the TMCs. The results illustrate that the phase compositions are Ti, TiB, and TiC, which confirm that the (TiB + TiC) reinforced TMCs have been prepared utilizing the *in situ* melting synthesis from Ti, B_4C, and C powders. The results also indicate that interfaces are clean and well bonded without

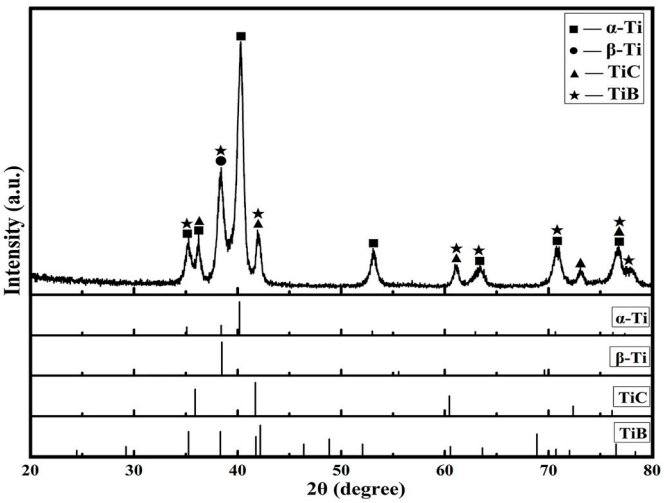

Fig. 1. X-ray diffraction patterns of the cast samples.

other useless reaction side products.

The material designation and the reinforcement volume fraction of the composites are displayed in Table 1. The microstructure of the *in situ* synthesized (TiB + TiC) enhanced TMCs with various volume fractions of reinforcements show that the volume fraction of (TiB + TiC) reinforcements increase with increasing B_4C and C powder contents, as shown in Fig. 2. As these reactions occur, there are clear changes of both the spherical TiC and needle-like TiB particles. The TiC morphology is revealed to change with a variation in the TiC volume fraction. With 1 vol % TiC, TiC particles are mainly short rods, but the TiC rod size increases with the rise of content [Fig. 2(a)]. When 3% TiC is added to the alloy, no rod-shaped TiC particles are observed, and equiaxial TiC dominates the main component [Fig. 2(c)]. When the TiC content is 4–5%, the quantity of the dendrite-shaped TiC gradually increases [Fig. 2(d)]. In a likewise manner, the size of the needle-like TiB increases with increasing TiB volume fraction, reaching a maximum at a content of 3%. Based on results, reinforcements are uniformly distributed throughout the alloy when the (TiB + TiC) volume fraction is 6% [Fig. 2(c)].

Fig. 3 shows the EPMA elemental maps of TMCs-3. The results show that reinforcements in these TMCs are mainly composed of needle-like TiB and spherical TiC particles. Confirmation of the reinforced phase structures also validates that the reactions of $5Ti + B_4C \rightarrow 4TiB + TiC$ and $Ti + C \rightarrow TiC$, have carried out completely during the *in situ* synthesis of Ti, B_4C, and C powders. The reinforced phases synthesized by in-situ method have better bonding than that formed by addition method, and is not easy to crack around them [35].

The microstructures of TMCs-3 are analyzed by EBSD. The inverse pole figure (IPF), grain-boundary (GB) maps, grain size and misorientation angle are shown in Fig. 4. The GB maps [Fig. 4(a)] show that small angle boundaries (2–15°) are marked in red, large angle boundaries (>15°) are in blue. Fig. 4(b) indicates that the volume percentage of the [0001]-oriented grains is very large, the [011$\bar{1}$0]-oriented grains are very few, and the distributions of the [$\bar{1}$2$\bar{1}$0] and [0001] oriented grains are relatively uniform. The average grain size of the primary alpha is about 12 μm [Fig. 4(c)]. It is analyzed from Fig. 4(d) that the proportion of small-angle grain boundaries is relatively low, while

Table 1
Review of the selected studies examined the tribological properties of composites for brake disk.

Ref.	Main materiel	Counter-body material	Wear condition				Wear properties	
			Applied Load (MPa)	Sliding speed (m/s)	Sliding Time (min)	p_0v	μ	Specific wear rate ($10^{-7}mm^3/Nmm$)
Present Work	Ti6Al4V	Cr12MoV	8	0.11	30	0.88	0.330	6.81
	TMCs-1 2 TiB + TiC (vol%)						0.324	5.34
	TMCs-2 4						0.272	4.22
	TMCs-3 6						0.264	4.06
	TMCs-4 8						0.274	4.19
	TMCs-5 10						0.241	3.47
[23]	6% vol% (TiC + TiB)/TC4 composite (TMCs-3)	Cr12MoV	12	0.22	10	2.64	0.316	3.58
				0.55		6.6	0.331	2.74
				1.10		13.2	0.322	4.81
			24	0.22		5.28	0.282	2.40
				0.55		13.2	0.327	8.21
				1.10		26.4	0.428	77.8
		GCr15	12	0.22		2.64	0.576	3.84
				0.55		6.6	0.285	5.34
				1.10		13.2	0.457	3.41
			24	0.22		5.28	0.398	1.99
				0.55		13.2	0.355	9.10
				1.10		26.4	0.421	57.5
[24]	5 wt% TiC/TiAl	Tungsten carbide (WC)	0.8	0.2	20	0.16	0.282	2.6
				0.9		0.72	0.331	4
	10 wt% TiC/TiAl			0.2		0.16	0.332	3.6
				0.9		0.72	0.353	3.3
[25]	CermeTi composite (5 TiB)	Jurid 539	1	2, 6, 9.6 and 15		2, 6, 9.6 and 15	0.25 (2 m/s)*	149**
							0.36 (9.6 m/s)*	
	CermeTi composite (10 TiC)						0.26 (2 m/s)*	104**
							0.30 (9.6 m/s)*	
	CermeTi composite (W TiC)						0.29 (2 m/s)*	81.9**
							0.31 (9.6 m/s)*	
[24]	Gray cast iron	Tungsten carbide	0.8	0.2	20	0.16	0.213	4.4
				0.9		0.72	0.328	16
[25]		Jurid 539	1	2, 6, 9.6, 15		2, 6, 9.6, 15	0.47 (2 m/s)*	23.6**
							0.34 (9.6 m/s)*	
[43]	3 wt% RM-AlHMMC***	EN32	0.5	3.14	13	1.57	0.35	9.33
	11 wt% RM-AlHMMC***						0.33	6.10

* Friction coefficient corresponding to sliding speed. ** cumulative wear after repeated drags at 4 different speeds. *** Redmud particle reinforced Al6061/Alumina/Graphite Hybrid Metal Matrix Composite (RM-AlHMMC).

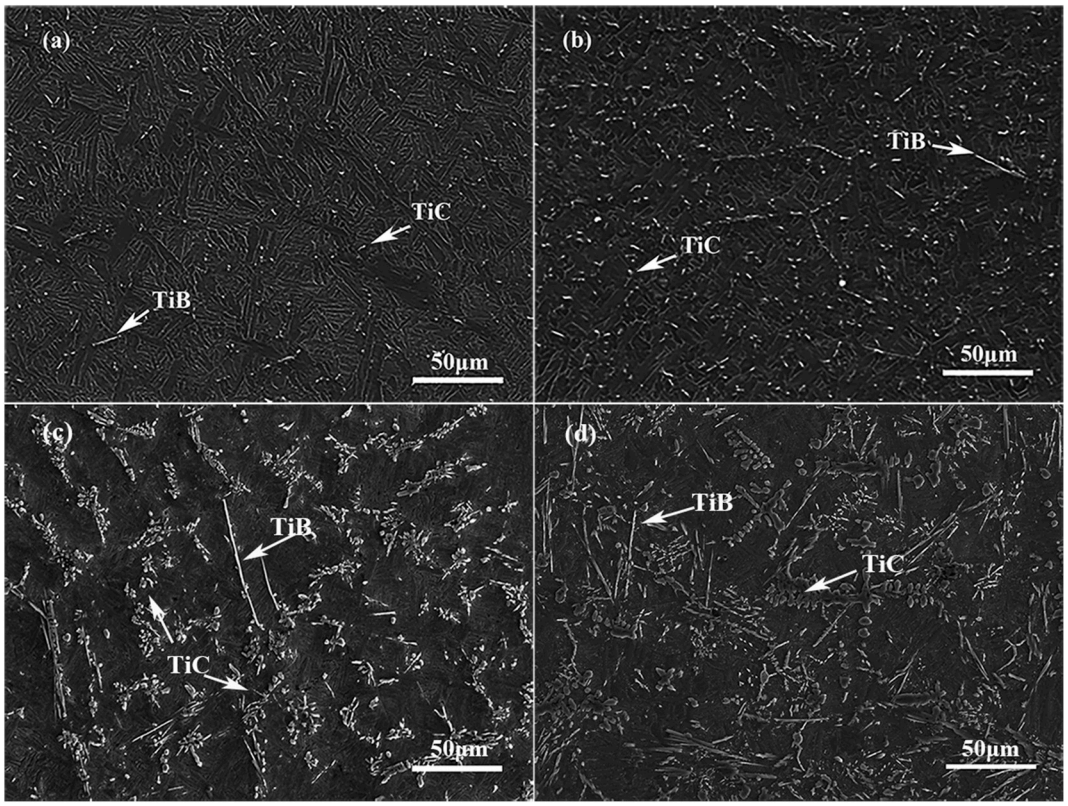

Fig. 2. Microstructures of (TiB + TiC) reinforced TMCs: (a) TMCs-1, (b) TMCs-2, (c) TMCs-3, and (d) TMCs-5.

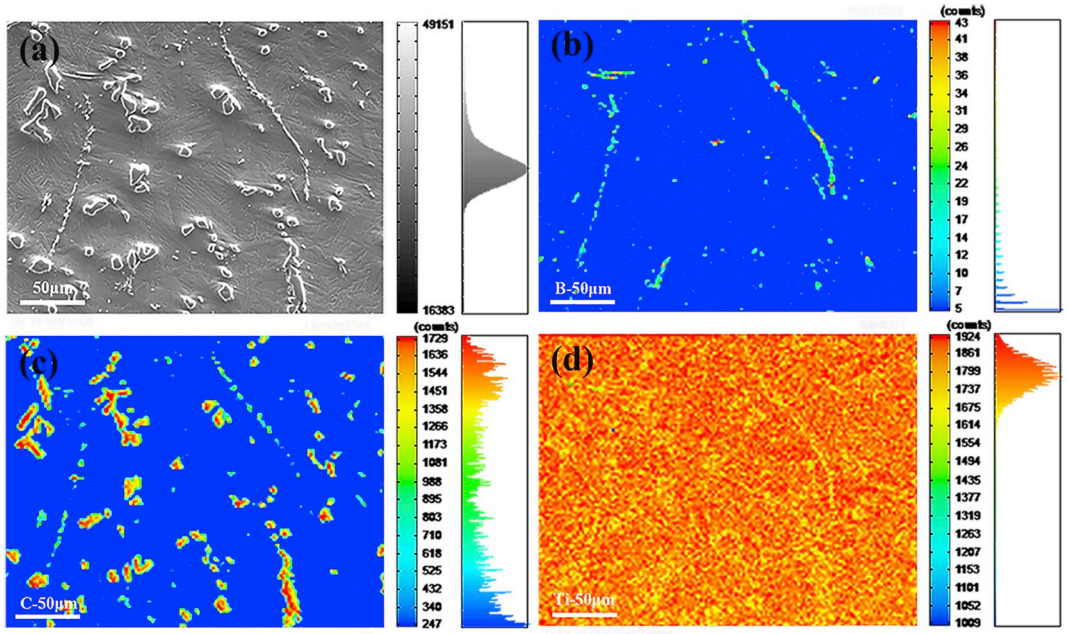

Fig. 3. EPMA elemental maps of TMCs-3.

that of large angle grain boundaries is very high. The small-angle grain boundary is encircled by the large-angle grain boundary. Usually, the region surrounded by large-angle grain boundaries represents a grain, which is a primary α phase or α + β cluster. The large-angle grain boundary is the grain boundary between the primary α phase and β transformation α + β cluster, and between different orientations of the α phase cluster and α + β cluster.

3.2. Friction and wear properties

Fig. 5(a) shows the coefficient of friction (COF) of Ti6Al4V and various TMCs at the normal load of 100 N. The coefficient of friction declines from 0.330 to 0.241 with the reinforcement content increases. It indicates that the COF in the steady-state stage of the curves varies with the reinforcement volume fraction, decreasing with the increased reinforcement volume fraction. The run-in time exhibits variations for

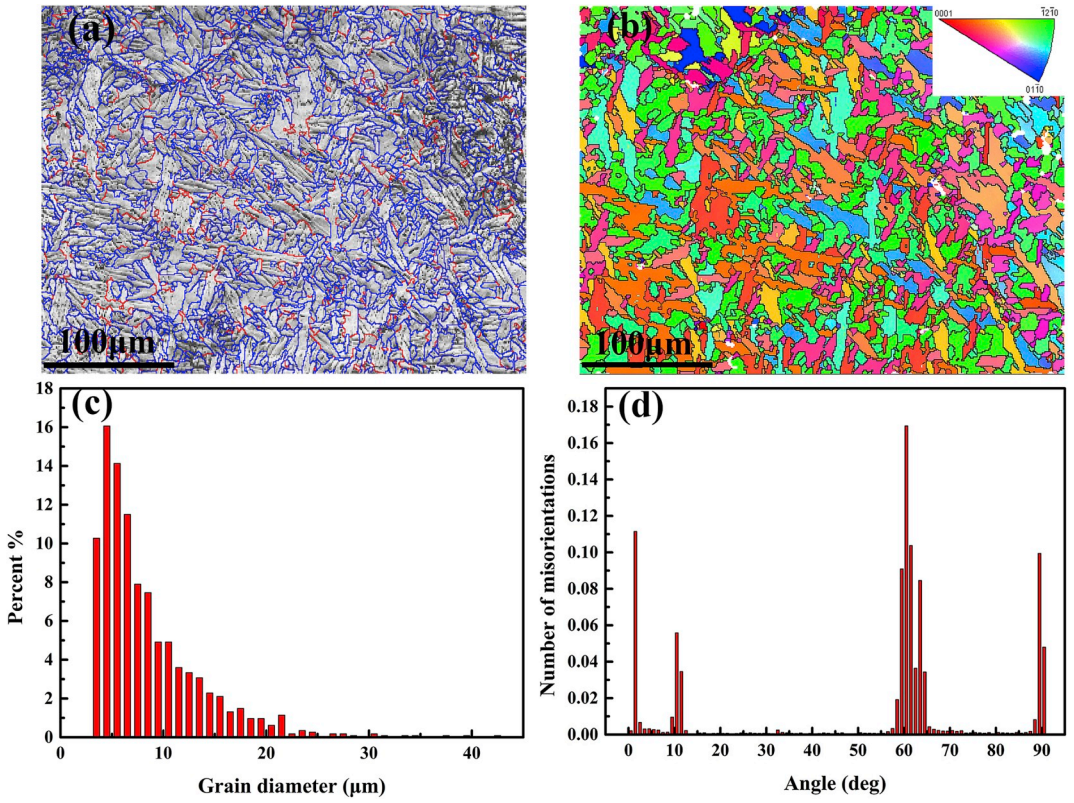

Fig. 4. EBSD analysis of TMCs-3: (a) The GB, (b) IPF maps, (c) Grain diameter, (d) Number fraction of grain boundaries with different angles of the microstructures.

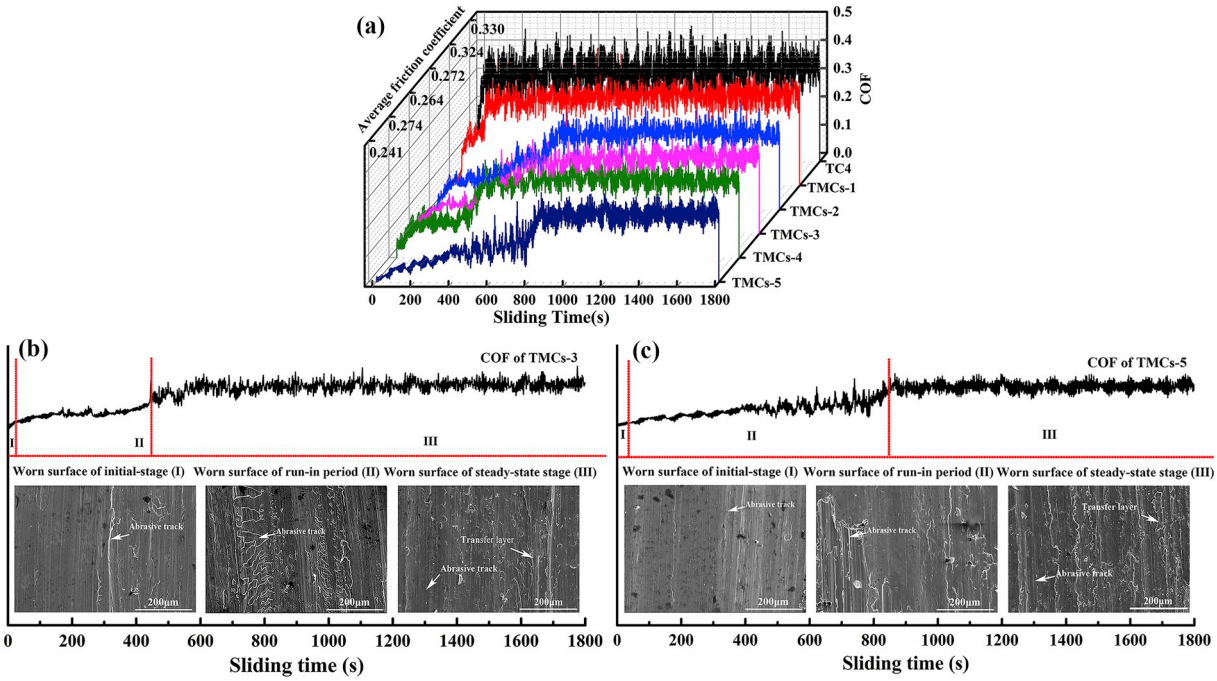

Fig. 5. Friction coefficients and worn surfaces of Ti6Al4V and TMCs under an applied load of 100 N. (a) Friction coefficients, (b) TMCs-3 at different stages, (c) TMCs-5 at different stages.

all COF statistics, and the length of the run-in period changed with the reinforcement volume fraction. Fig. 5(b) and (c) display the worn surface of TMCs-3 and TMCs-5 at different stages, respectively. In the initial stage, the wear degree of TMCs-5 is slightly lower than that of TMCs-3. However, more abrasive tracks on the worn surface of TMCs-3 are observed during the run-in period than those in the initial stage, which indicates that the roughness of the worn surface increased gradually to cause a rise in COF. Moreover, the worn surface of TMCs-5 is smoother than that of TMCs-3 in the run-in period, indicating that alloys with more reinforcements possesses better wear resistance. In addition, the

time required to form a stable transfer layer at the worn surface increases as particle debris accumulates during friction testing. The transfer layer can be recognized as being consist of worn particles and oxides, reinforcements, and matrix material [33]. With a reinforcement volume fraction of 10%, the roughness of the worn surface increases slowly owing to the high wear resistance. Thus, the run-in time is longer than that of a lower volume fraction. Under a normal load of 100 N, the worn surface of Ti6Al4V easily produces plastic deformation and is readily oxidized by the friction-generated heat. However, the heat-resistant and thermal stability of TMCs are found to be better than Ti6Al4V. Hence, it can be concluded that the varied run-in periods have resulted from the existence of reinforcements.

Fig. 6 displays the variation of Rockwell hardness and specific wear rates of TMCs. It shows that Rockwell hardness increases as the volume fraction increases. The hardness of TMCs-5 was greater than that of Ti6Al4V. Improving the hardness degree is a critical factor for enhancing the wear resistance, especially its abrasion resistance [36]. The results showed that TMCs harnesses increase with the addition of (TiB + TiC) reinforcements, which effectively enhance abrasion resistance under friction conditions. Wear loss is found to vary inversely with the reinforcement volume fraction.

Measurements of the specific wear rates of TMCs and Ti6Al4V show that TMCs wear losses decrease as (TiB + TiC) reinforcements increase, which indicates that these TMCs possess the higher wear resistance than Ti6Al4V [Fig. 6]. In addition, the specific wear rate of TMCs-3, in the steady friction region decreases by nearly 40%, compares with that of Ti6Al4V. The amount of wear experienced by the alloy can be predicted from friction tests. However, TMCs-5, and especially TMCs-3 and TMCs-4, exhibit little change in wear when the same friction parameters are used in testing. This result can be explained using the Archard theory [37].

$$Q = \frac{W}{3\sigma s} \tag{2}$$

where Q is the total wear, W the normal load, and σ_s the yield limit. Considering the probability, K, and sliding distance, L, a material's adhesive wear amount is expressed as:

$$Q = K\frac{WL}{3\sigma s} \tag{3}$$

In the case of elastic materials, H is the material hardness, and the expansion formula is

$$Q = K\frac{WL}{H} \tag{4}$$

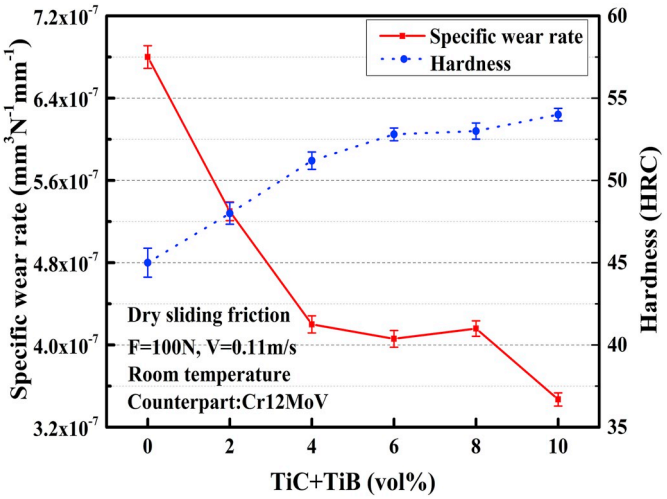

Fig. 6. The variation of Rockwell hardness and specific wear rates of TMCs.

where K is the adhesive wear coefficient. It can be inferred from this expression that higher hardness values results in a lower COF, which translate into less material wear.

Fig. 7 displays micrographs of worn surfaces of Ti6Al4V and TMCs. It reveals that many cutting and furrow marks are observed on worn surfaces of Ti6Al4V and TMCs, which indicates the existence of the adhesive wear and plastic deformation. When the volume fraction of (TiB + TiC) is 0–4%, the wear resistance is enhanced by the (TiB + TiC) reinforcement formation and coherent wear, such that the grinding, cutting, and furrow marks on these sample surfaces are less pronounced, which is a clear indication of the improved composite wear resistance [Fig. 7(a-c)]. Moreover, some short cracks are clearly observed on worn surfaces of Ti6Al4V. Almost no cracks appears in TMCs surfaces, which indicates that crack propagation behaviors have been stopped by reinforcements. Reinforcements significantly reduced abrasion and improved the wear resistance of the composites. Wear debris on worn surfaces is found to consist of fine particles that has broken free from surfaces of TMCs and Cr12MoV steel. Furthermore, these wear debris, adhered to sliding surfaces, may have degraded the contact area mechanical properties, ultimately resulting in higher wear rates.

When the volume fraction of (TiB + TiC) is 6–10%, the shapes of TiC particles appear to change from equiaxial to dendritic because of composition undercooling. The TiB particles retain their short-fiber shape, and the effects of TiB whiskers on the deformation resistance of the substrate alloy are greater because of pinning at grain boundaries. During the wear process, particles break from the alloys and settle on wear surfaces to form transition layers. These transfer layers appear to consist of flinty particles including the detached oxide debris, reinforcements, and substrate materials, which contain the elements, Ti, O, and Fe, and prevent the direct contact with the frictional pairs that results in the third body abrasion on contact surfaces [Fig. 7(d-f)]. During wear, pressure is concentrated at the contact region, leading to high temperatures and pressures. Added (TiB + TiC) reinforced phases in such titanium alloys can significantly increase high-temperature strengths. However, the effects of reinforcements on alloy strengths are not evident in this content range of 6–10%. Composite hardnesses are greater, and their shear resistances are better, such that the composite wear mechanism is primarily abrasive wear and slight adhesion, and material loss occurs mainly through plowing and breakage. During wear, adhesive and deformation portions of the wear mechanism are reduced due to the greater hardness, such that the plowing component of wear play a major role. As the TMCs surface hardness increases, the widths of surface scratches from wear decrease and occur regardless of the TiC particle size.

Fig. 8 shows stereomicroscopy images of the disc specimens against (a) Ti6Al4V, (b) TMCs-1, (c) TMCs-3, and (d) TMCs-5. It is found that the wear degree of the disk surface is different against various materials, and the deeper furrow and severe adhesive wear exist on the worn surface against Ti6Al4V corresponding to the wear morphology in Fig. 7(a). Owing to the low surface strength of Ti6Al4V, it is easy to accumulate a large amount of friction heat on the contact surface, resulting in adhesive wear. As the reinforcements increase, the furrow depths gradually decrease, and degree of adhesive wear reduces. The change law is in accordance with that of the worn pins. Almost no adhesive wear is observed, and only slight furrows exist on the worn surface of TMCs-5, which manifest that the main wear mechanism is the slight abrasive wear.

Fig. 9 and Table 2 display the EDS analysis results of the abrasive track and transfer layer of Ti6Al4V and TMCs-3. The main wear mechanisms of the Ti6Al4V alloy are severe adhesive and oxidative wear, but the TMCs-3 exhibits wear mechanisms that appear to be mild abrasive wear, adhesive wear, and oxidation wear.

Fig. 10 shows the cross-sections of worn surfaces, consisting of the transfer layer and reinforcements. When the volume fraction of (TiB + TiC) is 0–4%, TMCs surface hardnesses are not sufficient to resist wear,

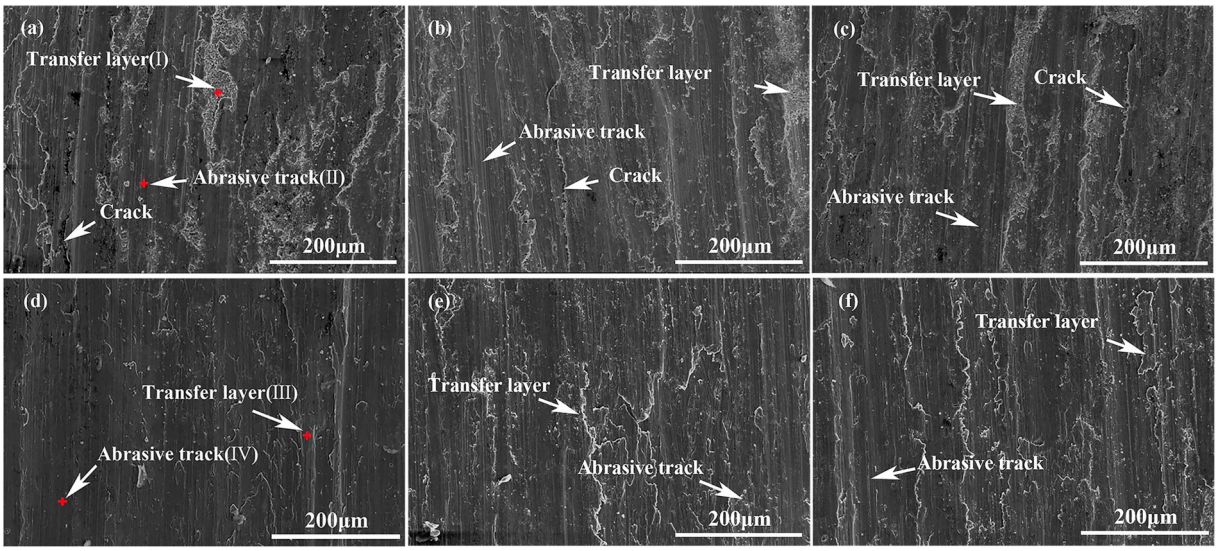

Fig. 7. Wear tracks of (a) Ti6Al4V, (b) TMCs-1, (c) TMCs-2, (d) TMCs-3, (e) TMCs-4, and (f) TMCs-5, under an applied load of 100 N.

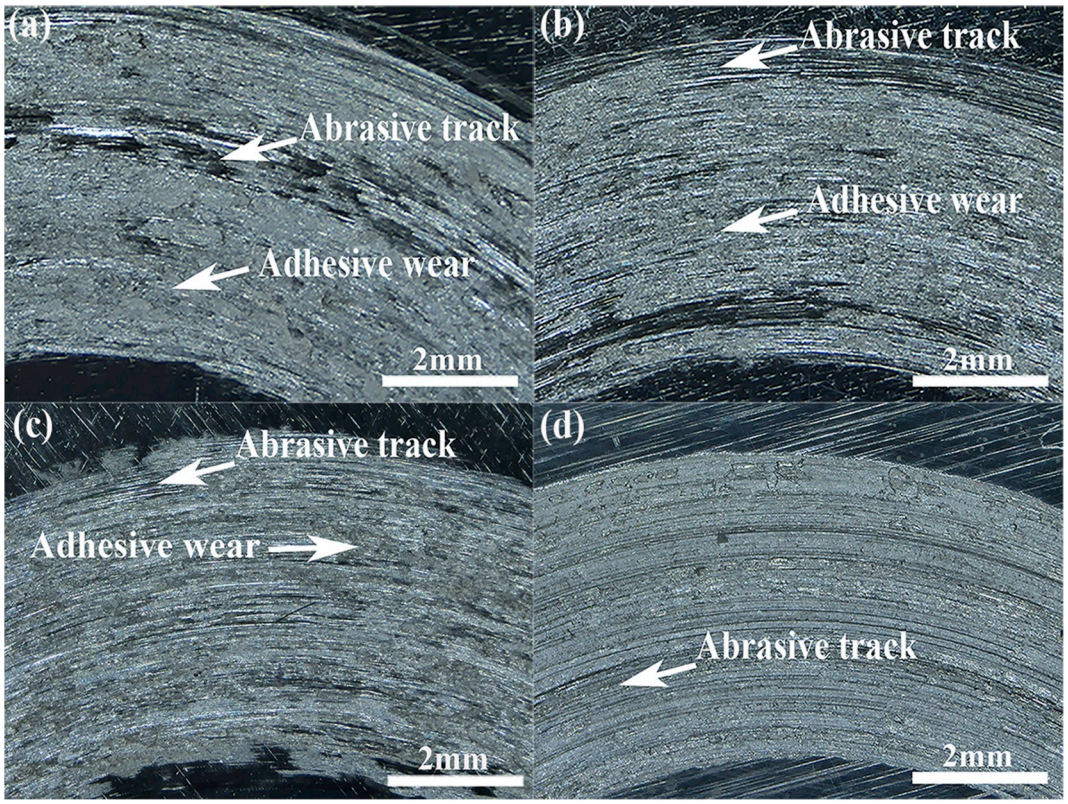

Fig. 8. Stereomicroscopy images of the disc specimens of (a) Ti6Al4V, (b) TMCs-1, (c) TMCs-3, and (d) TMCs-5.

such that the wear loss is caused by the adhesive wear between frictional pair surfaces. The main wear mechanisms are severe adhesive, and oxidative wear due to the low surface strength and friction-generated high temperature [Fig. 10(a-b)]. At the volume fraction of 6–10%, high hardness and abrasion-resistant (TiB + TiC) particles reduce abrasion and improve composite abrasion resistance by preventing flinty abrasion debris from being pressed into composite surfaces, the fracture energy of deformation and breakage can be absorbed by the exposed (TiB + TiC) reinforcements [Fig. 10(c-d)]. Fig. 10(e–f) indicate the exposed (TiB + TiC) reinforcements by local enlarged diagrams.

Figs. 11 and 12 show the EPMA elemental mapping images of Ti6Al4V and TMCs-3 under a normal load of 100 N. The present experimental results indicate that dispersed (TiB + TiC) reinforcements increase matrix metal hardnesses and possess good wear resistances. Moreover, the transfer layers are noted to consist primarily of B and C, with some Fe (Fig. 12). The 6–10 vol% (TiB + TiC) reinforced TMCs are more likely to form harder transfer layers than the 0–4 vol% reinforced TMCs, with the former being more capable of deformation resistance than the latter. Because of the presence of a hard transfer layer, COF decreases, and the wear amounts reduce.

Figs. 13 and 14 show the XPS survey spectra of the worn surfaces of Ti6Al4V and TMCs-3, respectively. The wide XPS spectra [Fig. 13(a)]

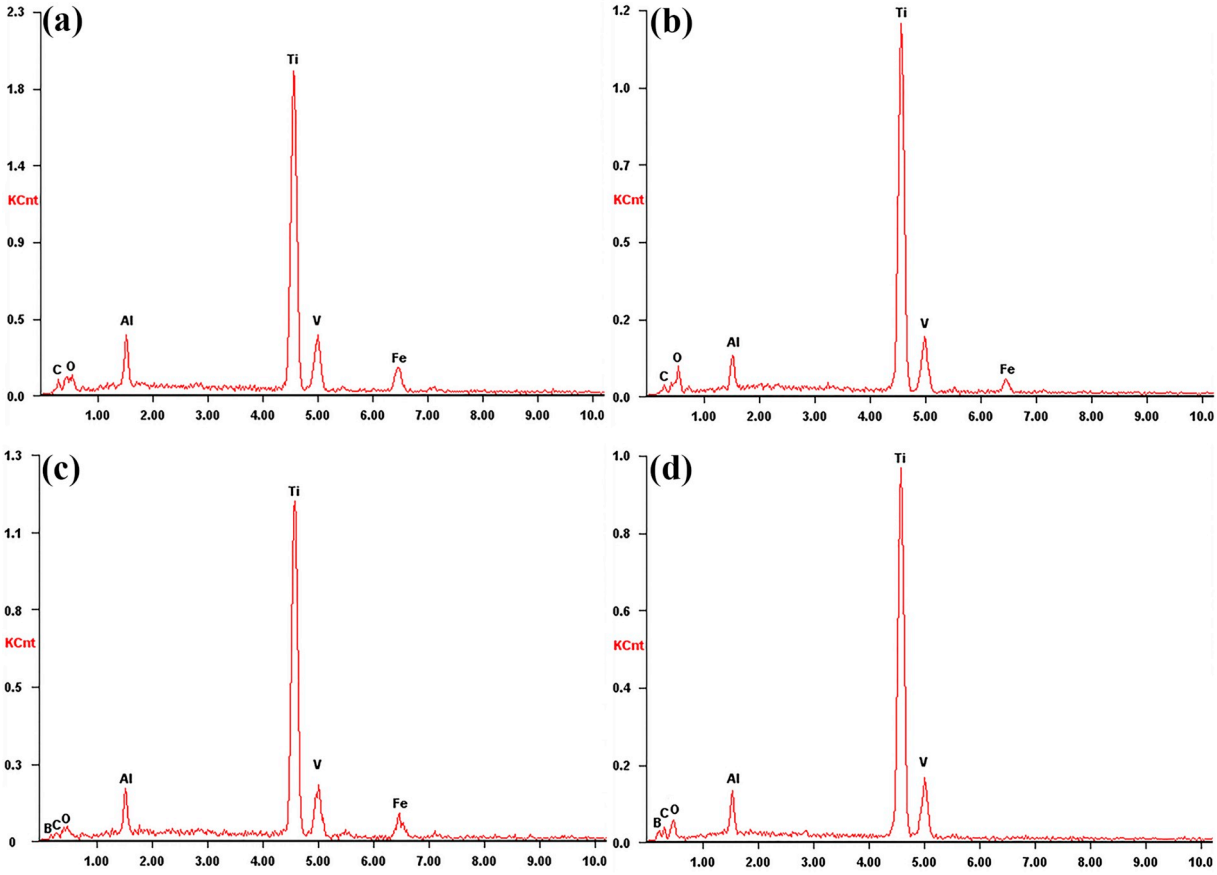

Fig. 9. EDS analysis of (a) transfer layer (I) and (b) abrasive track (II) of Ti6Al4V and the (c) transfer layer (III), and (d) abrasive track (IV) TMCs-3.

Table 2
EDS analysis of the abrasive track and transfer layer of Ti6Al4V and TMCs-3.

Specimen	Position	Composition (at.%)						
		O	Fe	C	B	Ti	Al	V
Ti6Al4V	Transfer layer (I)	24.61	10.23	3.07	0	55.84	4.24	2.01
	Abrasive track (II)	20.09	6.54	4.63	0	63.23	3.96	1.55
TMCs-3	Transfer layer (III)	10.16	5.96	12.49	10.47	55.51	3.29	2.12
	Abrasive track (IV)	3.89	0	16.75	14.65	60.26	2.66	1.79

show that the worn surface of Ti6Al4V pin composed of C 1s, O 1s, Fe 2p, and Ti 2p. In Fig. 13(b), the Fe doublets indicate that peak located at the binding energy of 710.55 eV corresponds to FeO, while peak at 724.14 eV accords with Fe_2O_3. With regard to the XPS of Ti 2p [Fig. 13(c)], the binding energies of Ti 2p3/2 and Ti 2p1/2 are 458.23 and 463.93 eV, respectively, which conform to the metallic Ti (Ti $^{[Me]}$) in the substrate. The splitting value between the two different peaks is about 5.7 eV, which further confirms that Ti on the worn surface primarily consist of the Ti^{4+} chemical state. Fig. 13(d) elucidates that the O 1s peaks are resolved into 529.58, 530.21 and 531.57 eV, which correspond to TiO_2, FeO and Fe_2O_3 respectively.

The narrow scan spectrum of the worn surface of TMCs-3 pin [Fig. 14 (b-d)] exhibits similar results. These TiO_2, FeO, and Fe_2O_3 oxides are still formed on the worn surface of TMCs-3. However, the content of these oxides is different from that of the surface without reinforcements. The XPS survey spectra show a lower intensity of oxygen, iron, and titanium in Fig. 14(a) than that in Fig. 13(a), indicating that the adhesion wear and oxidative wear during the sliding process decrease on the worn surface. After adding reinforcement phases, the content of Fe decreases by nearly half, which indicates that the strength of the material is improved, and the degree of adhesion wear is reduced. This XPS results are consistent with the previous EDS analysis, which indicate that the addition of reinforcements can improve the adhesion wear resistance.

4. Discussion

Abrasive wear on the worn surface can arise from various wear mechanisms, such as the shear wear, plastic deformation, and fatigue wear [38,39]. The overall hardness is not a single evaluation of the material-wear resistance. Instead, the wear performance is a comprehensive event affected by a variety of factors. In fact, the homogeneity of the material and the wear surface state have significant impacts on the wear resistance.

For the research concerning the effects of the microstructure and worn surface state on wear properties, the microstructure and the wear properties of the (TiB + TiC) reinforced Ti matrix composites are studied by means of SEM, EPMA, XRD, EBSD, and XPS. For (TiC + TiB) hybrid reinforced composites, the addition of (TiC + TiB) reinforcements at the same time has a certain influence on each other. The existence of TiB restrains the growth of TiC and makes TiC particles smaller with increasing TiB content. With the increase of the reinforced phase content, the matrix structure is refined, and the reinforced phases distribute

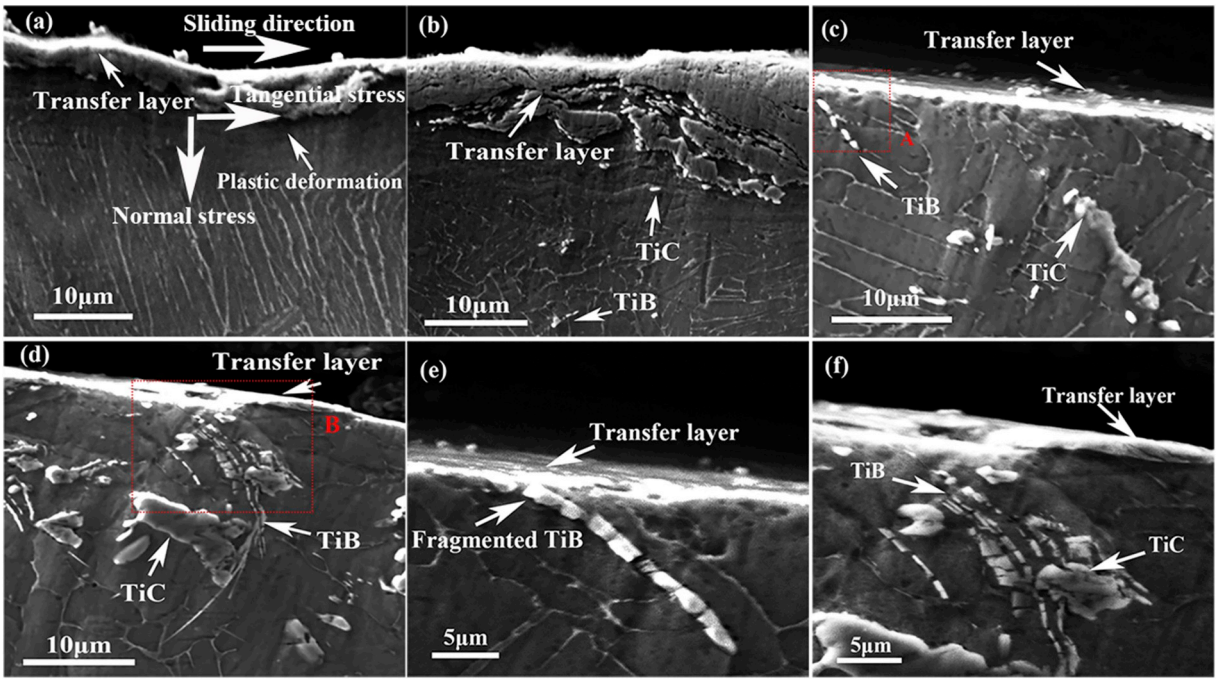

Fig. 10. Cross-section of the wear track of (a) Ti6Al4V, (b) TMCs-1, (c) TMCs-2, and (d) TMCs-3, (e) Magnified image of (c)-A region, and (f) Magnified image of (d)-B region.

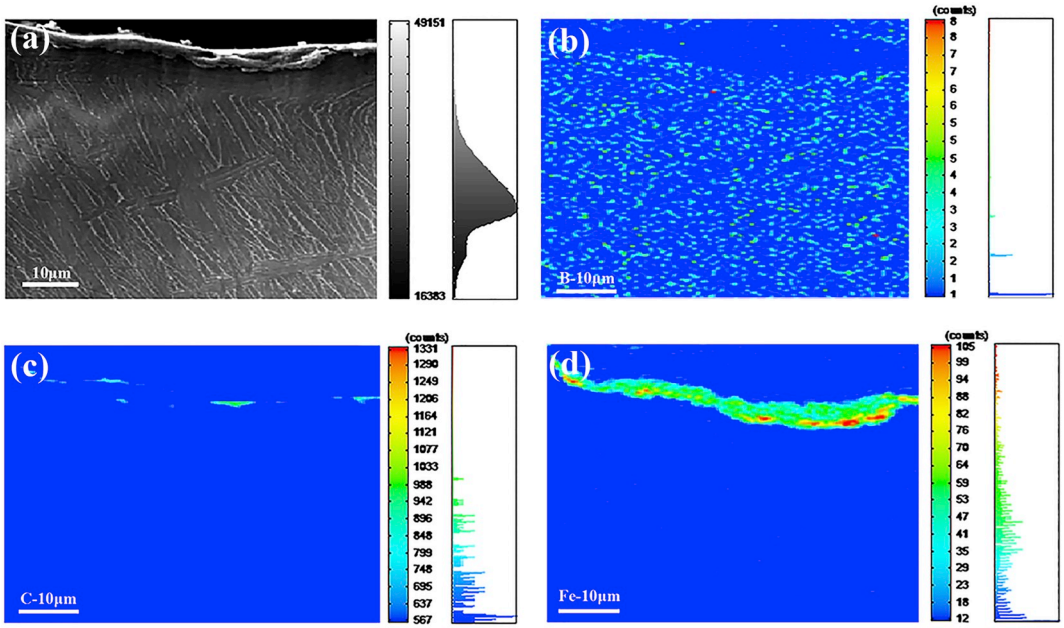

Fig. 11. EPMA elemental mapping images of Ti6Al4V under an applied load of 100 N.

evenly in the matrix, which play the role of dispersion strengthening. In particular, the results of the EPMA, EBSD analysis show that the reinforced phases and matrix of TMCs-3 have good microstructures (Figs. 2 and 4). It is found that the worn surfaces can be characterized by the abrasive track, surface oxidation, and transfer layer due to the adhesion and removal of the metallic/oxide debris by the reciprocal movement of the contact surface (Figs. 7 and 9). This trend is the major formation mechanism of the transfer layer in particle-reinforced TMCs. In addition, the cross-section of the abrasion track indicates that the uniform distribution of reinforced phases in the matrix has a certain effect on dispersion strengthening to improve the ability to resist the surface shear stress. Hence, this effect is enough to enhance the sub-surface strength and hardness of the TMCs and prevent the initiation of microcracks during sliding. On the other hand, the reinforcements are prominent in the matrix due to the delamination occurring on the worn surface during wear, which prevent the direct contact between the matrix and the friction disc. Moreover, the hard reinforcements act as the load-bearing role owing their higher strength, hardness and modulus than the matrix. Under the same friction condition, the wear rate and COF decrease with the reinforcements increase (Fig. 6). Moreover, the morphology of the reinforcement has a great influence on the wear resistance. The fine TiC particles are easier to fall off from the matrix

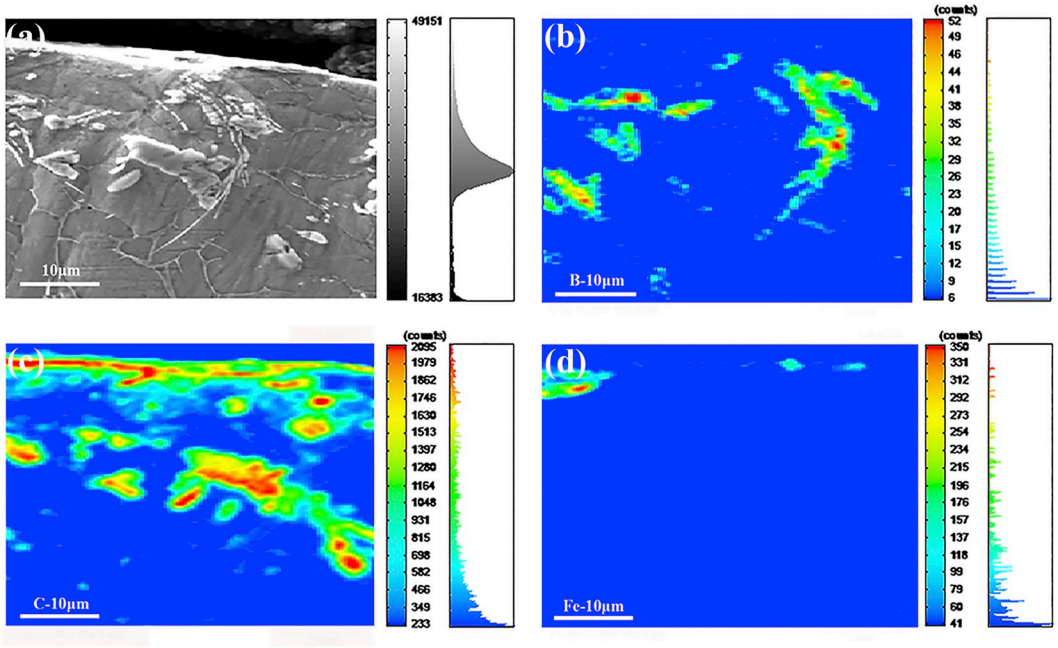

Fig. 12. EPMA elemental mapping images of TMCs-3 under an applied load of 100 N.

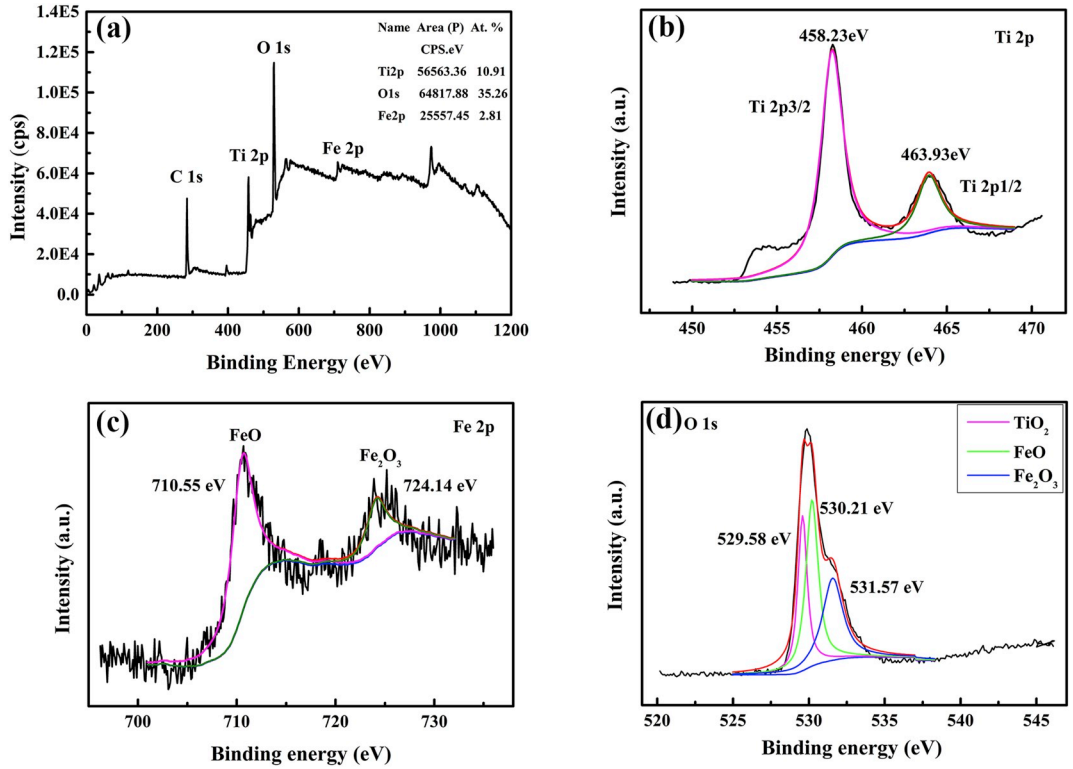

Fig. 13. XPS spectra of Ti6Al4V worn pin (a) wide scan, XPS peak fitting of (b) Fe 2p, (c) Ti 2p, and (d) O 1s.

than equiaxed TiC particles due to the effect of the shear force during the wear process, which causes the wear-resistance degradation (Fig. 10). The binding force of the slender needle-like TiB is stronger than short the needle-like TiB, and possesses better pinning effects.

The interface changes from the initial metal-to-metal contact to the metal-to-oxide contact during the sliding process. The surface of Ti6Al4V is prone to be severe adhesion and oxidation wear at the interface under the high pressure due to the surface-heat softening effect. However, the worn surface of TMCs-3 is ascribed to forming a dense and stable transfer layer according to the EPMA, EDS, and XPS analysis results (Figs. 9–14), which prevents the direct mutual action of contact surfaces and evidently restrains the friction fluctuations. Moreover, the matrix Ti, reinforcements, TiO_2, FeO, and Fe_2O_3 are detected on the worn surfaces. The variation of the Fe content transferred from the friction disc reflects the degree of adhesive wear during wear. With the worn surface temperature rises, the Ti and Fe elements on the surface

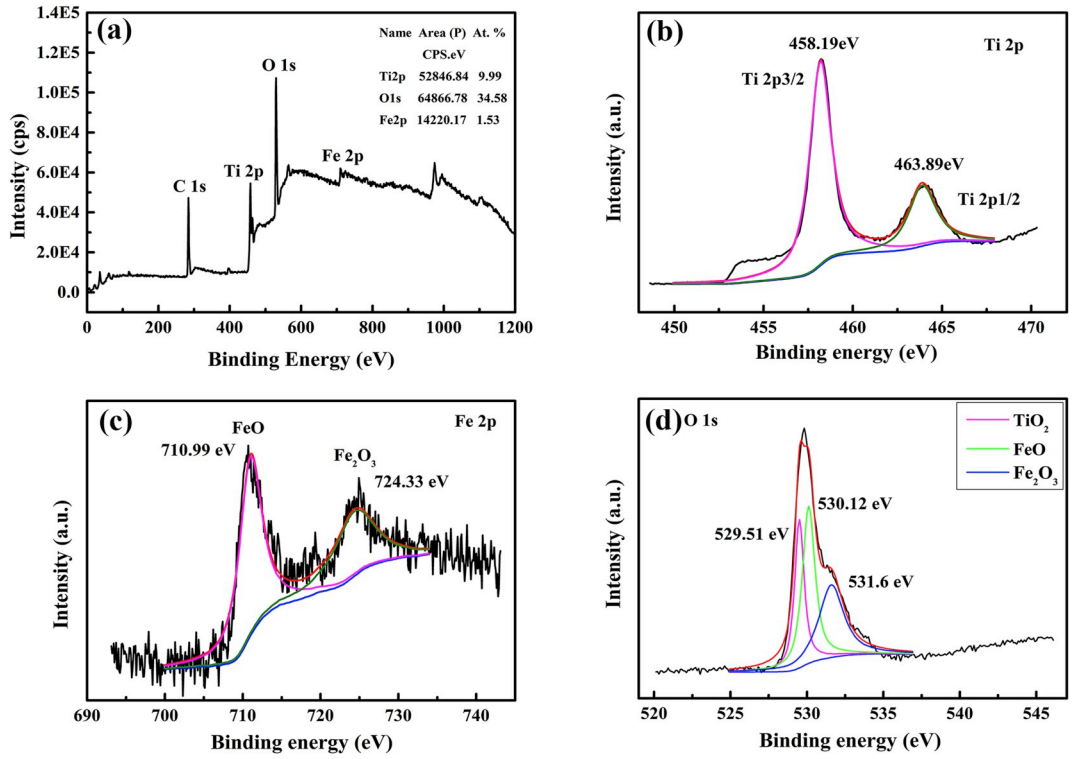

Fig. 14. XPS spectra of TMCs-3 worn pin (a) wide scan, XPS peak fitting of (b) Fe 2p, (c) Ti 2p, and (d) O 1s.

are easily oxidized, causing the formation of oxides. With increasing the reinforcements, the oxide content decreases and the oxidation wear are weakened.

To further illustrate that TMCs have good potential applications for brake disc usages, the previous research results on the tribological performances of metal matrix composites under different conditions are listed in Table 1. In real brake systems, the friction performance is affected by the sliding speed, v, and nominal contact pressure, p_o, so the $p_o v$ value is usually considered as the coefficient to evaluate the friction condition and usually changes from 0.3 to 20 MPa m/s [40,41]. Thus, to meet the service conditions of brake discs, the nominal contact pressure p_o selected in this paper is 8 MPa, and the sliding speed v is 0.11 m/s, then the $p_o v$ value is 0.88 MPa m/s. Moreover, the previous results of our group show that the $p_o v$ values are between 2.6 and 26.4 MPa m/s [23], which accord with an appropriate range to study the tribological characteristics of these materials. As seen from Table 1, the coefficient of friction is effected by the factors such as normal load, sliding speed, and the contact material. In addition, the coefficient of friction of TMCs is in a specific range ($0.25<\mu<0.55$) conforming to the J standards from the society of automotive engineers procedures-SAE [42]. Compared with redmud particle reinforced Al6061/alumina/graphite hybrid metal matrix composite (RM-AlHMMC) [43], the specific wear rates of TMCs are lower than them even in higher $p_o v$ value conditions [23], and they are also superior to the traditional gray cast iron [24,25] under similar $p_o v$ value conditions regardless of the contact material. Although the strength of TiAl alloy as matrix is higher than Ti6Al4V, the TMCs represent the same level of wear resistance of the TiC/TiAl composite under higher $p_o v$ value conditions, which indicate that the (TiB + TiC) hybrid reinforced may be better than single TiC enhanced. Hence, the tribological properties of TMCs display excellent performance, which indicate the possibility of using it as a candidate for a lightweight brake disc to replace the heavier gray cast iron.

As a summary, tribological properties of TMCs are enhanced owing to the uniform distribution of TiC and TiB reinforcements, which strengthen the surface shear resistance. Moreover, only by forming a dense and stable transfer layer can the interface be protected, thus increasing the wear resistance of the TMCs. The effect of the composite strength is of equal importance with contact-surface states. The composites exhibit the excellent friction performance when both factors are in a well-controlled condition.

5. Conclusions

The high stress and speed friction properties of TMCs pins against Cr12MoV disks were studied under dry conditions with special emphasis on the relationship between microstructure evolutions and wear-surface states. The main findings are as follows:

1. Particulate-reinforced TMCs were fabricated by casting Ti6Al4V alloys containing needle-like TiB and spherical TiC particles that were prepared by *in situ* reactions among Ti, B_4C, and C powders. The TiC morphology gradually changed from granular and equiaxial to dendritic morphologies, and the existence of TiB restrained the growth of TiC and made TiC particles smaller with increasing TiB content. The matrix structure was refined, and the (TiB + TiC) reinforced phases were distributed evenly in the matrix, which played a critical role in dispersion strengthening and improving the wear and shear deformation resistance.
2. As the (TiB + TiC) reinforcements volume fraction increased, TMCs hardness increased and the degree of wear reduced in friction tests. Friction transfer layers, which consisted of worn particles containing reinforcements, FeO, TiO_2, and Fe_2O_3, prevented the direct contact between the frictional pairs, thus reducing the COF and wear rate.
3. The fine TiC particles are easier to fall off from the matrix than equiaxed TiC particles due to the effect of the shear force during wear, and the binding force of the slender needle-like TiB is stronger than short the needle-like TiB, and possesses better pinning effects.
4. This dense and stable transfer layer reduced the shear strength on the surfaces of the friction pairs and limited the direct interaction of contact surfaces, thus improving the wear resistance of the TMCs. As the reinforcement content of composites increased, the main wear

mechanism altered from the severe adhesive and oxidative wear to slight adhesive, abrasive, and oxidative wear.

Declaration of competing interestCOI

We declare that we have no financial and personal relationships with other people or organizations that can inappropriately influence our work, there is no professional or other personal interest of any nature or kind in any product, service and/or company that could be construed as influencing the position presented in, or the review of, the manuscript entitled.

CRediT authorship contribution statement

Bowen Zheng: Conceptualization, Methodology, Validation, Investigation, Data curation, Writing - original draft, Visualization. **Fuyu Dong:** Formal analysis, Writing - review & editing, Supervision, Funding acquisition. **Xiaoguang Yuan:** Project administration, Funding acquisition. **Hongjun Huang:** Resources. **Yue Zhang:** Supervision. **Xiaojiao Zuo:** Resources. **Liangshun Luo:** Funding acquisition. **Liang Wang:** Funding acquisition. **Yanqing Su:** Funding acquisition. **Weidong Li:** Writing - review & editing. **Peter K. Liaw:** Writing - review & editing, Funding acquisition. **Xuan Wang:** Funding acquisition.

Acknowledgments

This work is supported the National Key Research and Development Program of China (2016YFB0301201), and Major Science and Technology Special Plan of Yunnan (2018ZE013), Foundation of Liaoning Province Education Administration (LQGD2019001), Natural Science Foundation of Liaoning Province (20180510056, 2019-ZD-0216), National Natural Science Foundation of China (51401129, 51871075, 51875365, 51901029), Project funded by China Postdoctoral Science Foundation (2019M653337). PKL thanks the support from the National Science Foundation (DMR-1611180 and 1809640) with the program directors, Drs G. Shiflet and D. Farkas.

References

[1] Attar H, Ehtemam-Haghighi S, Kent D, Dargusch MS. Recent developments and opportunities in additive manufacturing of titanium-based matrix composites: a review. Int J Mach Tool Manuf 2018;133:85–102. https://doi.org/10.1016/j.ijmachtools.2018.06.003.

[2] Zhang CJ, Qu JP, Wu J, Zhang SZ, Han JC, Hayat MD, Cao P. A titanium composite with dual reinforcements of micrometer sized TiB and submicrometer sized Y_2O_3. Mater Lett 2018;233:242–5. https://doi.org/10.1016/j.matlet.2018.09.012.

[3] Obadele BA, Andrews A, Olubambi PA, Mayhew MT, Pityana S. Effect of ZrO_2, addition on the dry sliding wear behavior of laser clad Ti6Al4V alloy. Wear 2015;328–329:295–300. https://doi.org/10.1016/j.wear.2015.02.056.

[4] Mo JL, Zhu MH. Tribological investigation of WC/C coating under dry sliding conditions. Wear 2011;71:1998–2005. https://doi.org/10.1016/j.wear.2010.12.016.

[5] Zhu L, Petrova RS, Gashinski JP, Yang Z. The effect of surface roughness on PEO-treated Ti-6Al-4V alloy and corrosion resistance. Surf Coat Technol 2017;325:22–9. https://doi.org/10.1016/j.surfcoat.2017.05.044.

[6] Huang C, Zhang Y, Rui V, Shen JY. Dry sliding wear behavior of laser clad TiVCrAlSi high entropy alloy coatings on Ti-6Al-4V substrate. Mater Des 2012;41:338–43. https://doi.org/10.1016/j.matdes.2012.04.049.

[7] Farayibi PK, Murray JW, Huang L, Bond F, Kinnell PK, Clare AT. Erosion resistance of laser clad Ti-6Al-4V/WC composite for waterjet tooling. J Mater Process Technol 2014;214:710–21. https://doi.org/10.1016/j.jmatprotec.2013.08.014.

[8] Sun SY, Wang MM, Wang LQ, Qin JN, Lu WJ, Zhang D. The influences of trace TiB and TiC on microstructure refinement and mechanical properties of in situ synthesized Ti matrix composite. Compos B Eng 2012;43:3334–7. https://doi.org/10.1016/j.compositesb.2012.01.075.

[9] Sun SY, Wang LQ, Qin JN, Chen YF, Lu WJ, Zhang D. Microstructural characteristics and mechanical properties of in situ synthesized (TiB+TiC)/TC18 composites. Mater Sci Eng A 2011;530:602–6. https://doi.org/10.1016/j.msea.2011.10.029.

[10] Sahoo BN, Panigrahi SK. Synthesis, characterization and mechanical properties of in-situ (TiC-TiB_2) reinforced magnesium matrix composite. Mater Des 2016;109:300–13. https://doi.org/10.1016/j.matdes.2016.07.024.

[11] Wen Y, Guo TT, Zhou YG, Bai HP, Wang Z. Nanoindentation characterization on microhardness of micron-level TiC and TiB reinforcements in in-situ synthesized (TiC+TiB)/Ti-6Al-4V composite. Front Mater 2019. https://doi.org/10.3389/fmats.2019.00205.

[12] Ni DR, Geng L, Zhang J, Zheng ZZ. Fabrication and tensile properties of in situ, TiBw and TiCp hybrid-reinforced titanium matrix composites based on Ti-B_4C-C. Mater Sci Eng A 2008;478:291–6. https://doi.org/10.1016/j.msea.2007.06.004.

[13] Hattal A, Chauveau T, Djemai M, Fouchet JJ, Bacroix B, Dirras G. Effect of nano-yttria stabilized zirconia addition on the microstructure and mechanical properties of Ti6Al4V parts manufactured by selective laser melting. Mater Des 2019;180:107909. https://doi.org/10.1016/j.matdes.2019.107909.

[14] Huang X, Gao YM, Wang ZP, Yi YL, Wang YR. Microstructure, mechanical properties and strengthening mechanisms of in-situ prepared (Ti_5Si_3+$TiC_{0.67}$)/TC4 composites. J Alloy Comp 2019;792:907–17. https://doi.org/10.1016/j.jallcom.2019.04.056.

[15] Mo JL, Zhu MH. Tribological investigation of WC/C coating under dry sliding conditions. Wear 2010;271:1998–2005. https://doi.org/10.1016/j.wear.2010.12.016.

[16] Sivananth V, Vijayarangan S, Rajamanickam N. Evaluation of fatigue and impact behavior of titanium carbide reinforced metal matrix composites. Mater Sci Eng A 2014;597:304–13. https://doi.org/10.1016/j.msea.2014.01.004.

[17] Li SF, Kondoh K, Imai H, Chen B, Jia L, Umeda J. Microstructure and mechanical properties of P/M titanium matrix composites reinforced by in-situ, synthesized TiC-TiB. Mater Sci Eng A 2015;628:75–83. https://doi.org/10.1016/j.msea.2015.01.033.

[18] Min YK, Park JS, Min KP, Kim KT, H Hong S. Effect of aspect ratios of in situ formed TiB whiskers on the mechanical properties of TiB_w/Ti-6Al-4V composites. Scr Mater 2012;66:487–90. https://doi.org/10.1016/j.scriptamat.2011.12.024.

[19] Huang LJ, Geng L, Peng HX. In situ (TiB_w+TiC_p)/Ti6Al4V composites with a network reinforcement distribution. Mater Sci Eng A 2010;527:6723–7. https://doi.org/10.1016/j.msea.2010.07.025.

[20] Zhang CJ, Sun YG, Chen YF, Lian YZ, Zhang SZ, Feng H, Zhou YW, Kong FT, Chen YY. Deformation behavior and microstructure evolution mechanism of 5vol.%(TiB_w+TiC_p)/Ti composites during isothermal compression. Mater Char 2019;154:212–21. https://doi.org/10.1016/j.matchar.2019.06.002.

[21] Geng L, Ni DR, Zhang J, Zheng ZZ. Hybrid effect of TiBw and TiCp on tensile properties of in situ titanium matrix composites. J Alloy Comp 2008;463:488–92. https://doi.org/10.1016/j.jallcom.2007.09.054.

[22] Ni DR, Geng L, Zhang J, Zheng ZZ. Fabrication and tensile properties of in situ TiBw and TiCp hybrid-reinforced titanium matrix composites based on Ti–B 4 C–C. Mater Sci Eng A 2008;478:291–6. https://doi.org/10.1016/j.msea.2007.06.004.

[23] Zheng BW, Dong FY, Yuan XG, Zhang Y, Huang HJ, Zuo XJ, Luo LS, Wang L, Su YQ, Wang X, Cheng J. Insights into wear behavior of (TiC+TiB)/TC4 composites against different counterface materials. Mater Res Express 2019;6:116584. https://doi.org/10.1088/2053-1591/ab4bac.

[24] Liaquat H, Shi XL, Yang K, Huang YY, Liu XY, Wang ZH. Tribological behavior of TiAl metal matrix composite brake disk with TiC reinforcement under dry sliding conditions. J Mater Eng Perform 2017;26:3457–64. https://doi.org/10.1007/s11665-017-2789-1.

[25] Blau PJ, Jolly BC, Qu J, Peter WH, Blue CA. Tribological investigation of titanium-based materials for brakes. Wear 2007;263:1202–11. https://doi.org/10.1016/j.wear.2006.12.015.

[26] Wang L, Li XX, Zhou Y, Zhang QY, Chen KM, Wang SQ. Relations of counterface materials with stability of tribo-oxide layer and wear behavior of Ti-6.5Al-3.5Mo-1.5Zr-0.3Si alloy. Tribol Int 2015;91:246–57. https://doi.org/10.1016/j.triboint.2015.01.028.L.

[27] Wang L, Zhang QY, Li XX, Cui XH, Wang SQ. Severe-to-mild wear transition of titanium alloys as a function of temperature. Tribol Lett 2014;53:511–20. https://doi.org/10.1007/s11249-013-0289-5.

[28] Cai W, Bellon P, Beaudoin AJ. Probing the subsurface lattice rotation dynamics in bronze after sliding wear. Scr Mater 2019;172:6–11. https://doi.org/10.1016/j.scriptamat.2019.07.002.

[29] An Q, Huang LJ, Bao Y, Zhang R, Jiang S, Geng L, Xiao MM. Dry sliding wear characteristics of in-situ TiBw/Ti6Al4V composites with different network parameters. Tribol Int 2018;121:252–9. https://doi.org/10.1016/j.triboint.2018.01.053.

[30] Mao YS, Wang L, Chen KM, Wang SQ, Cui XH. Tribo-layer and its role in dry sliding wear of Ti-6Al-4V alloy. Wear 2013;297:1032–9. https://doi.org/10.1016/j.wear.2012.11.063.

[31] Österle W, Deutsch C, Gradt T, Orts-Gil G, Schneider T, Dmitriev AI. Tribological screening tests for the selection of raw materials for automotive brake pad formulations. Tribol Int 2014;73:148–55. https://doi.org/10.1016/j.triboint.2014.01.017.

[32] Wang Y, Li J, Dang C, Wang Y, Zhu Y. Influence of carbon contents on the structure and tribocorrosion properties of TiSiCN coatings on Ti6Al4V. Tribol Int 2017;109:285–96. https://doi.org/10.1016/j.triboint.2017.01.002.

[33] Choi BJ, Kim IY, Lee YZ, Kim YJ. Microstructure and friction/wear behavior of (TiB+TiC) particulate-reinforced titanium matrix composites. Wear 2014;318:68–77. https://doi.org/10.1016/j.wear.2014.05.013.

[34] Huttunen-Saarivirta E, Kilpi L, Hakala TJ, Metsäjoki J, Ronkainen H. Insights into the behaviour of tool steel-aluminium alloy tribopair at different temperature. Tribol Int 2018;119:567–84. https://doi.org/10.1016/j.triboint.2017.11.041.

[35] Choi BJ, Kim YJ. In-Situ (TiB+TiC) particulate reinforced titanium matrix composites: effect of B_4C size and content. Met Mater Int 2013;6:1301–7. https://doi.org/10.1007/s12540-013-6024-9.

[36] Viáfara CC, Sinatora A. Unlubricated sliding friction and wear of steels: an evaluation of the mechanism responsible for the T1, wear regime transition. Wear 2011;271:1689–700. https://doi.org/10.1016/j.wear.2010.12.085.

[37] Lijesh KP, Khonsari MM. On the modeling of adhesive wear with consideration of loading sequence. Tribol Lett 2018;66:105. https://doi.org/10.1007/s11249-018-1058-2.
[38] Farahnaz H, Abbas ZH, Hamid RA, Dalibor P, Barthab K. The subsurface frictional hardening: a new approach to improve the high-speed wear performance of Ti-29Nb-14Ta-4.5Zr alloy against Ti-6Al-4V extra-low interstitial. Wear 2019; 422–423:137–50. https://doi.org/10.1016/j.wear.2018.12.095.
[39] Huttunen-Saarivirta E, Kilpi L, Hakala TJ, Metsajoki J, Ronkainen H. Insights into the behaviour of tool steel-aluminium alloy tribopair at different temperatures. Tribol Int 2018;119:567–84. https://doi.org/10.1016/j.triboint.2017.11.041.
[40] Straffelini G, Pellizzari M, Molinari A. Influence of load and temperature on the dry sliding behaviour of Al-based metal-matrix-composites against friction material. Wear 2004;256:754–63. https://doi.org/10.1016/s0043-1648(03)00529-5.
[41] Chandra Vermaa P, Menapacea L, Bonfantib A, Ciudina R, Gialanellaa S, Straffelinia G. Braking pad-disc system: wear mechanisms and formation of wear fragments. Wear 2015;322–323:251–8. https://doi.org/10.1016/j.wear.2014.11.019.
[42] Kchaou M, Sellami A, Fajoui J, Kus R, Elleuch R, Jacquemin Frédéric. Tribological performance characterization of brake friction materials: what test? What coefficient of friction? Proc Inst Mech Eng J J Eng Tribol 2018;233:214–26. https://doi.org/10.1177/1350650118764167.
[43] Kumar M, Megalingam A. Tribological characterization of Al6061/alumina/graphite/redmud hybrid composite for brake rotor application. Part Sci Technol 2019;37:261–74. https://doi.org/10.1080/02726351.2017.1367747.